

Internal structure and its connection with thermodynamics and dynamics in black holes

Yan-Gang Miao* and Hao Yang†

School of Physics, Nankai University, Tianjin 300071, China

Abstract

In general, a finite metric function at the center of a black hole describes a non-singular spacetime but an infinite metric at the center gives a singular spacetime, where the former is associated with convergent Ricci and Kretschmann scalars together with complete radial geodesics, while the latter is related to divergent Ricci and Kretschmann scalars together with incomplete radial geodesics. For the charged black hole in the four-dimensional Einstein-Gauss-Bonnet theory, we find that its metric function is finite at its center in one region of parameters but complex in the other region of parameters. The finite case describes a strange spacetime which presents the Ricci and Kretschmann scalars of a singular spacetime and the radial geodesics of a non-singular spacetime, while the complex case gives rise to the similar situation. We verify that the cosmic censorship conjecture is maintained for the black hole model. Further, we investigate the second-order phase transition, quasinormal modes of perturbation of a test scalar field in the eikonal limit, and shadow radius for the black hole and find that the thermodynamic and dynamic properties depend on the metrics. In this way, we connect the internal structure with the thermodynamics and dynamics for this black hole. Moreover, we compare such a black hole of modified gravity with the Reissner-Nordström black hole of Einstein's general relativity in these thermodynamic and dynamic properties.

*Corresponding author. E-mail address: miaoyg@nankai.edu.cn

†E-mail address: yanghao4654@mail.nankai.edu.cn

1 Introduction

Traditionally, Lovelock's theorem has shown [1] that Einstein's general relativity is the unique theory of gravity in the four-dimensional spacetime if the diffeomorphism invariance, metricity, and second order equations of motion are required. However, from the point of view of conformal gravity, the Einstein-Gauss-Bonnet (EGB) theory in four dimensions, the so-called 4D EGB gravity, was given [2] with conformal anomaly and developed [3] with Gauss-Bonnet entropic corrections. Recently, it was rediscovered [4] by the way of starting with a higher dimensional EGB theory, rescaling the EGB parameter and taking the limit of the spacetime dimension to four. Later, a lot of related studies have been done, which can roughly be classified into three types. The first type of research mainly focuses on the extension of the 4D EGB gravity, such as constructing the charged black hole [5], the Bardeen black hole [6], the noncommutative inspired black hole [7], and the Born-Infeld black hole [8], *etc.* The second type of the relevant studies argues the self consistency of the strategy adopted in Ref. [4] and of the theory itself on various aspects, for instance, field equations and Lagrangians [9], instability of vacua [10], and some other criticisms [11]. Furthermore, a well-defined 4D gravity theory was proposed [12, 13] from the Horndeski scalar-tensor theory and from a minimally modified gravity theory, respectively. The last type of research reveals [14] new interesting properties of the 4D EGB gravity in dynamics and thermodynamics of black holes, in particular, quasinormal modes and shadows [15], and restrictions to the EGB parameter from the observations of M87* [16] and the speed of gravitational waves measured by GW170817 and GRB 170817A [17], and from validity of the weak cosmic censorship conjecture [18], *etc.*

The charged 4D EGB black hole can be divided [2, 5] into two classes depending on the positivity or negativity of the EGB parameter,¹ where the metric function with the positive parameter is complex at the center, while the metric function with the negative parameter is real and finite when the negative parameter and the charge satisfy a certain constraint. In general, if a metric function is finite at the center of a black hole, it describes a non-singular spacetime in which the Ricci and Kretschmann scalars are convergent and the radial geodesics are complete; but if a metric function is infinite at the center, it gives a singular spacetime in which the Ricci and Kretschmann scalars are divergent and the radial geodesics are incomplete. Here we point out that the charged 4D EGB black hole is an exception. The metric function of this black hole is finite everywhere for the negative EGB parameter plus its constraint to the charge, but it describes a strange spacetime in which the Ricci and Kretschmann scalars are divergent, however, the radial geodesics are complete, which is quite amazing because the Ricci and Kretschmann scalars present the properties of a singular spacetime but the radial geodesics show the properties of a non-singular spacetime. For the positive EGB parameter, the metric function of this black hole takes a complex value at its center, and the resulting spacetime has similar properties of curvature invariants and radial geodesics to those in the case of the negative EGB parameter.

Due to the peculiarity of the charged 4D EGB black hole, we further investigate how the finite and complex metric functions result in different thermodynamic and dynamic effects. We focus on the

¹We make a note that the EGB parameter is positive or negative in different cases. If the causality of the bulk structure in the AdS space is imposed [19], the EGB parameter should be negative; if no superluminal sound speed of gravitational waves is required [20] in the stochastic gravitational wave background, the EGB parameter should be positive.

second-order phase transition, the quasinormal modes of perturbation of a test scalar field in the eikonal limit, and shadow radius. In addition, considering that the charged 4D EGB black hole turns back to the Reissner-Nordström (RN) black hole in the limit of vanishing EGB parameter, we compare the charged 4D EGB black hole with the RN black hole in these thermodynamic and dynamic properties and then obtain some interesting relations.

The second-order phase transition point of black holes was first found by Davies [21], known as “the Davies point”. When a black hole evolves past the Davies point, the sign of its heat capacity changes, indicating that the black hole has undergone a phase transition. As the heat capacity diverges at the Davies point, the phase transition is second order. The Davies points exist in the RN black hole and the Kerr black hole, but not in the Schwarzschild black hole whose heat capacity is always negative. We pointed out [22] that the Davies point appears in the uncharged 4D EGB black hole. Here we shall further investigate the behaviors of Davies points for the charged 4D EGB black hole.

Quasinormal modes provide [23] a characteristic variable of dynamics to depict the ringdown phase of black hole mergers, where their real parts correspond to the oscillating frequency of perturbations, while their imaginary parts to the damping time. Normally the quasinormal modes can only be computed numerically, but in the eikonal limit they can be derived [24] analytically, *i.e.*, the light ring/quasinormal mode correspondence, where the angular velocity of unstable null geodesics determines the real part of the quasinormal modes and the Lyapunov index does the imaginary part. Although this correspondence is not valid [25] for all field perturbations, it holds for our test scalar field. Besides the quasinormal modes, another important observable is the shadow radius of a black hole [26] which is inversely proportional to the real part of the quasinormal modes of perturbation of a test scalar field in the eikonal limit when observed at infinity. Thus, the quasinormal modes in the eikonal limit and the shadow radius represent the dynamic properties of the charged 4D EGB black hole.

This paper is organized as follows. In Sec. 2, we determine the constraints under which the metric function of the charged 4D EGB black hole is real and finite or complex at the center, and discuss the cosmic censorship conjecture for this black hole model. Next, we examine in Sec. 3 the behaviors of Davies points when the EGB parameter takes values in different ranges. We continue our discussions in Sec. 4 on the quasinormal modes of perturbation of a test scalar field in the eikonal limit. Finally, we give our conclusions in Sec. 5 where some comments and further extensions are included. We note that the term “complex metric function” only means the property at the center of black holes throughout this paper.

2 Charged 4D EGB black hole

The metric function of the charged 4D EGB black hole takes [2, 5] the form,

$$f_{\alpha}(r) = 1 + \frac{r^2}{2\alpha} \left[1 - \sqrt{1 + 4\alpha \left(\frac{2M}{r^3} - \frac{q^2}{r^4} \right)} \right], \quad (1)$$

where α stands for the EGB parameter, M the mass, and q the charge. Under the limit $\alpha \rightarrow 0$, the charged 4D EGB black hole turns back to the RN black hole with the metric function as follows,

$$f_{\text{RN}}(r) = 1 - \frac{2M}{r} + \frac{q^2}{r^2}. \quad (2)$$

By solving the algebraic equation, $f_\alpha(r) = 0$, one can obtain the event horizons of the charged 4D EGB black hole,

$$r_{\text{H}}^\pm = M \pm \sqrt{M^2 - q^2 - \alpha}. \quad (3)$$

The existence of horizons requires

$$M^2 - q^2 - \alpha \geq 0. \quad (4)$$

2.1 Complex metric function

When $r \rightarrow 0$, the asymptotic behavior of the term under the square root in Eq. (1) is

$$1 + 4\alpha \left(\frac{2M}{r^3} - \frac{q^2}{r^4} \right) \rightarrow -\frac{4\alpha q^2}{r^4}, \quad (5)$$

which means that the metric function takes a complex value if $\alpha > 0$. We notice that the complex metric function is different from the usual function that is infinite at the center of black holes. The appearance of a complex metric function is parameter dependent. Next, we investigate the Ricci scalar, the Kretschmann scalar, and the radial geodesic in the case of the positive EGB parameter.

2.1.1 Ricci scalar and Kretschmann scalar

It is well known that the divergence of Ricci and Kretschmann scalars reflects the existence of an irreducible singularity in spacetime. So it is obvious that the spacetime of charged 4D EGB black holes has singularity when the EGB parameter is positive, which can be seen clearly from the asymptotic form of the Ricci scalar in the limit of $r \rightarrow 0$,

$$\lim_{r \rightarrow 0} R \sim \frac{4iq}{r^2 \sqrt{\alpha}}, \quad (6)$$

and the asymptotic form of the Kretschmann scalar in the limit of $r \rightarrow 0$,

$$\lim_{r \rightarrow 0} K \sim -\frac{4q^2}{r^4 \alpha}. \quad (7)$$

2.1.2 Radial geodesic

For a spherically symmetric spacetime with the metric function $f(r)$, the radial time-like geodesic of a neutral particle satisfies [27]

$$\left(\frac{dr}{d\tau} \right)^2 + f(r) = E^2, \quad (8)$$

where τ is the proper time and E the total energy per unit mass, and $E^2 = 1$ corresponds to a free particle. Thus the square of radial velocities associated with τ of a free neutral particle is

$$v^2 \equiv \left(\frac{dr}{d\tau} \right)^2 = 1 - f(r). \quad (9)$$

First of all, let us review the incompleteness of the radial geodesic [28] in the uncharged 4D EGB black hole spacetime. The square of radial velocities of a neutral particle falling into the center of the black hole is

$$\left(\frac{dr}{d\tau} \right)^2 = E^2 - 1 + \sqrt{\frac{2M}{\alpha}} r^{1/2} + O(r^{3/2}). \quad (10)$$

Thus, this square is exactly zero when a free neutral particle reaches the center, resulting in the spacetime incompleteness.

Next, we calculate the square for a neutral particle falling into the center of the charged 4D EGB black hole when $\alpha > 0$,

$$\left(\frac{dr}{d\tau} \right)^2 = E^2 - 1 - \sqrt{-\frac{q^2}{\alpha}} + \sqrt{-\frac{q^2}{\alpha}} \cdot \frac{M}{q^2} r + O(r^2). \quad (11)$$

We can see that this square is imaginary for a free neutral particle ($E^2 = 1$) when $r \rightarrow 0$. This shows that no physical observer can reach the black hole center in a finite proper time. In addition, we compute the innermost radius that the particle can reach,

$$r_{\text{in}} = \frac{q^2}{2M}, \quad (12)$$

which is bigger than the critical radius r_b of the zone of the complex metric function.² Note that the zone within the innermost radius is unreachable, which implies that the zone of the complex metric function is unreachable, too.

2.2 Finite metric function

We continue our analyses of the metric function for the charged 4D EGB black hole by combining the function with the event horizons. At first, in order to have a real metric, we impose the constraint,

$$1 + 4\alpha \left(\frac{2M}{r^3} - \frac{q^2}{r^4} \right) \geq 0, \quad r \in [0, +\infty). \quad (13)$$

²According to Eq. (1), the critical radius of the zone of the complex metric function satisfies the equation: $r_b^4 + 8\alpha M r_b - 4\alpha q^2 = 0$, and the only real and positive solution can be obtained, $r_b = \sqrt{\frac{2\sqrt{2}\alpha M}{\sqrt{\sqrt[3]{4/9A} - 2\sqrt[3]{2/3}\alpha q^2/A}} - \left(\sqrt[3]{4/9A}/2 - \sqrt[3]{2/3}\alpha q^2/A\right) - \sqrt{\sqrt[3]{4/9A}/2 - \sqrt[3]{2/3}\alpha q^2/A}}$, where $A \equiv \sqrt[3]{\sqrt{3(27\alpha^4 M^4 + 4\alpha^3 q^6) + 9\alpha^2 M^2}}$. It is not easy to determine which is bigger, r_b or r_{in} . To this end, we introduce the function, $s(r) \equiv r^4 + 8\alpha M r - 4\alpha q^2$, and investigate its monotonicity. Because the derivative of $s(r)$ with respect to r is positive when $\alpha > 0$, i.e., $ds(r)/dr = 4r^3 + 8\alpha M > 0$, $s(r)$ is a monotonically increasing function. Further, considering $s(r_{\text{in}}) = \left(\frac{q^2}{2M}\right)^4$ and $s(r_b) = 0$, that is, $s(r_{\text{in}}) > s(r_b)$, thus we deduce $r_{\text{in}} > r_b$.

When $r > \frac{q^2}{2M}$, meaning $\frac{2M}{r^3} - \frac{q^2}{r^4} > 0$, the above condition becomes

$$\alpha \geq -\frac{r^4}{4(2Mr - q^2)} \equiv h(r). \quad (14)$$

Because $h(r)$ takes its maximum at $r_0 = \frac{2q^2}{3M}$,

$$h(r_0) = -\frac{4q^6}{27M^4}, \quad (15)$$

Eq. (14) gives the lower bound of α ,

$$\alpha \geq -\frac{4q^6}{27M^4}. \quad (16)$$

Moreover, when $0 < r < \frac{q^2}{2M}$, meaning $\frac{2M}{r^3} - \frac{q^2}{r^4} < 0$, Eq. (13) implies

$$\alpha \leq h(r). \quad (17)$$

Considering

$$\frac{dh(r)}{dr} = \frac{r^3(2q^2 - 3Mr)}{2q^2 - 2Mr^2} > 0, \quad (18)$$

and $h(r) \rightarrow 0$ when $r \rightarrow 0$, we can see that $h(r)$ increases monotonically in the range of $0 < r < \frac{q^2}{2M}$ and its minimum is zero. So, Eq. (17) gives the upper bound of α ,

$$\alpha \leq 0. \quad (19)$$

Combining Eq. (16) with Eq. (19), we get the constraint to α ,

$$-\frac{4q^6}{27M^4} \leq \alpha \leq 0, \quad (20)$$

which is just the requirement to maintain a real metric function.

In addition, we need to consider the restrictions from horizons, i.e. the existence of horizons, Eq. (4). For the case of $q^2 \leq M^2$, Eq. (4) does not give extra restrictions to Eq. (20), while for the case of $q^2 > M^2$, the combination of Eq. (4) and Eq. (20) leads to a more compact condition than Eq. (20),

$$-\frac{4q^6}{27M^4} \leq \alpha \leq M^2 - q^2. \quad (21)$$

Note that we shall verify this inequality soon later by checking $-\frac{4q^6}{27M^4} \leq M^2 - q^2$.

For the sake of concision in the following demonstrations, we introduce the rescaling of variables,

$$\frac{q}{M} \rightarrow Q, \quad \frac{\alpha}{M^2} \rightarrow a, \quad (22)$$

with which we rewrite the constraint conditions that consist of Eq. (20) and Eq. (21) in a dimensionless form,

$$-\frac{4}{27}Q^6 \leq a \leq 0, \quad \text{for } Q^2 \leq 1, \quad (23a)$$

$$-\frac{4}{27}Q^6 \leq a \leq 1 - Q^2, \quad \text{for } Q^2 > 1. \quad (23b)$$

Now we compensate the proof for the inequality Eq. (21) or its dimensionless form Eq. (23b), that is, to check $1 - Q^2 \geq -\frac{4}{27}Q^6$. To this end, we define a function,

$$g(Q) \equiv 1 - Q^2 + \frac{4}{27}Q^6, \quad (24)$$

and then prove $g(Q) \geq 0$ for $Q^2 > 1$. We draw the graph of $g(Q)$ with respect to Q in Fig. 1, from which we can finish our proof. We pay attention to the two zero points of $g(Q)$ located at $Q = \pm\sqrt{\frac{3}{2}}$, where a has one unique value, $a = -\frac{1}{2}$. This means that the charged 4D EGB black hole has only one horizon when the rescaled EGB parameter equals $-\frac{1}{2}$, i.e. the inner and outer horizons merge.

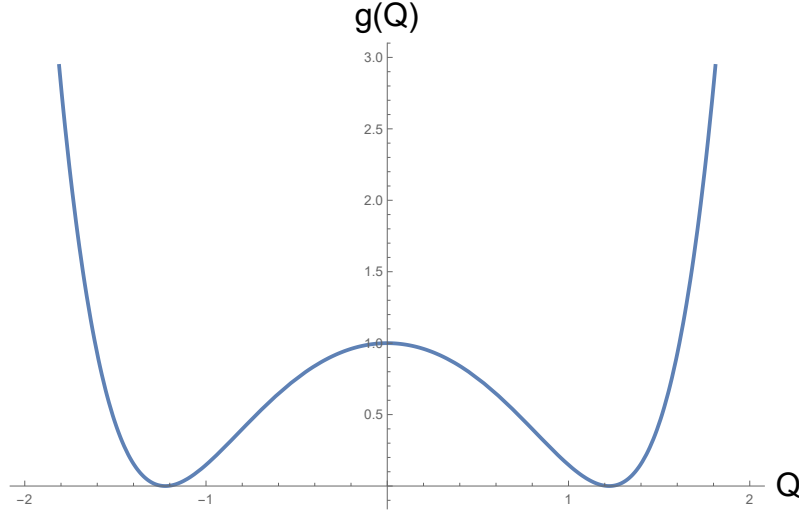


Figure 1: The function $g(Q)$ is tangent to the horizontal axis Q at the two points, $(\pm\sqrt{\frac{3}{2}}, 0)$.

Besides the rescaled charge and EGB parameter, see Eq. (22), we rescale the radial coordinate r by

$$\frac{r}{M} \rightarrow x, \quad (25)$$

and then rewrite the horizons Eq. (3) as

$$x_{\text{H}}^{\pm} = 1 \pm \sqrt{1 - Q^2 - a}, \quad (26)$$

where it seems that a takes the range from minus infinity to zero. In fact, there are no solutions for $f_{\alpha}(r) = 0$ if $a < -\frac{1}{2}$. Let us make a detailed analysis. It is obvious that the algebraic equation, $f_{\alpha}(r) = 0$, can be simplified to be

$$\sqrt{1 + 4\alpha \left(\frac{2M}{r^3} - \frac{q^2}{r^4} \right)} = 1 + \frac{2\alpha}{r^2}, \quad (27)$$

where the both hand sides should not be negative. However, the right hand side may be negative when $\alpha < 0$, which gives rise to an extra restriction to the range of α . In order to find out such an extra

condition, we substitute $r = r_{\text{H}}^+$ into the right hand side of Eq. (27) and thus obtain the extra constraint for α ,

$$1 + \frac{2\alpha}{\left(M + \sqrt{M^2 - q^2 - \alpha}\right)^2} \geq 0, \quad (28)$$

or its dimensionless form,

$$2a \geq -(1 + \sqrt{1 - Q^2 - a})^2. \quad (29)$$

It is obvious from Eq. (29) that the existence of horizons requires the condition, $a \leq 1 - Q^2$, which gives the upper bound,

$$a = 1 - Q^2, \quad (30)$$

see the red curve in Fig. 2. When a takes its minimum, $a_{\text{min}} = -\frac{1}{2}$, $|Q|$ takes its maximum, $|Q|_{\text{max}} = \sqrt{\frac{3}{2}}$. Moreover, Eqs. (23a) and (23b) determine the lower bound,

$$a = -\frac{4}{27}Q^6, \quad (31)$$

see the brown curve in Fig. 2. In other words, we can fix the physical region of Q and a by combining the constraints Eqs. (23a), (23b), and (29), and depict it in Fig. 2, where it is clear that $a < -\frac{1}{2}$ is beyond this physical region.

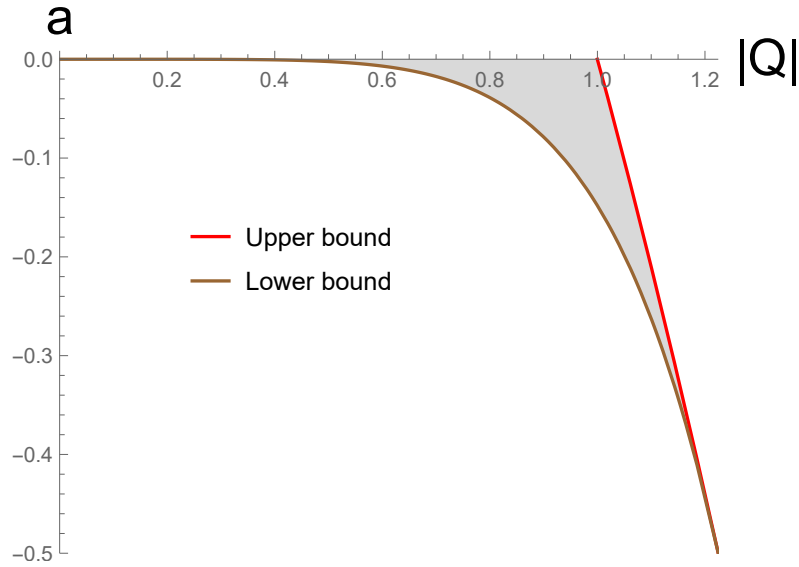


Figure 2: The horizontal axis denotes the absolute value of the rescaled charge $|Q|$ and the vertical axis the rescaled EGB parameter a . The shadow area determines the parameter region allowed by the set of constraints Eqs. (23a), (23b), and (29), in which the metric function is finite everywhere.

As a result, the metric function of the charged 4D EGB black hole is finite everywhere when $|Q|$ and a take values within the gray area in Fig. 2.

2.2.1 Ricci scalar and Kretschmann scalar

It is obvious that the spacetime of charged 4D EGB black holes has singularity when the EGB parameter is negative, which can be seen clearly from the asymptotic form of the Ricci scalar in the limit of $r \rightarrow 0$,

$$\lim_{r \rightarrow 0} R \sim -\frac{4q}{r^2 \sqrt{-\alpha}}, \quad (32)$$

and the asymptotic form of the Kretschmann scalar in the limit of $r \rightarrow 0$,

$$\lim_{r \rightarrow 0} K \sim -\frac{4q^2}{r^4 \alpha}. \quad (33)$$

2.2.2 Radial geodesic

We calculate the square of radial velocities of a neutral particle falling into the center of the charged 4D EGB black hole and find that it is same as Eq. (11) but it is associated with $\alpha < 0$. We can see that this square is negative for a free particle ($E^2 = 1$) when $r \rightarrow 0$. This shows that no physical observer can reach the black hole center in a finite proper time. Moreover, we note that the innermost radius that the particle can reach is same for the cases of $\alpha > 0$, $\alpha < 0$, and $\alpha \rightarrow 0$ (the vanishing case corresponds to the RN black hole) because Eq. (12) is independent of α .

We make a brief summary of this subsection. Whether the metric function of the charged 4D EGB black hole is complex ($\alpha > 0$) or real and finite ($\alpha < 0$) at the center of this black hole spacetime, the Ricci scalar is imaginary (Eq. (6)) or infinite (Eq. (32)), and the Kretschmann scalar is infinite (Eq. (7) and Eq. (33)), while the radial geodesics are complete. This presents the peculiarity of the curvature invariants of the charged 4D EGB black hole. We make a note that the peculiarity also appears in the complete radial geodesics, where the completeness is based on an imaginary velocity³ which never leads to a finite proper time for a free falling particle to reach the center.

2.3 Cosmic censorship conjecture

The cosmic censorship conjecture requires that the singularity in a black hole spacetime should always be surrounded by an event horizon in order to prevent a naked singularity from destroying the causal structure of the spacetime. We expect that the cosmic censorship conjecture is satisfied for the charged 4D EGB black hole. Here we shall use the Gedanken experiment [29] combined with the superradiation theory [30] to verify whether the cosmic censorship conjecture is maintained or not. The idea is to shoot a particle into the black hole and test whether the event horizon of this black hole will be destroyed. If the event horizon is destroyed, the cosmic censorship conjecture is violated; if not, the cosmic censorship conjecture is maintained. For the charged 4D EGB black hole with mass M_0 and charge q_0 , we know from Eq. (3) that the event horizon exists under the condition,

$$M_0^2 \geq q_0^2 + \alpha, \quad (34)$$

³Usually the completeness is based on an infinite proper time.

where the equal sign means the case of the extreme black hole. The black hole mass becomes $M_0 + \delta M$ and the charge $q_0 + \delta q$ after the black hole absorbs an incident scalar particle of frequency ω and charge q_s , where $\omega \ll M_0$ and $q_s \ll q_0$. Obviously, if the event horizon were destroyed, the mass and charge would satisfy

$$(M_0 + \delta M)^2 < (q_0 + \delta q)^2 + \alpha, \quad (35)$$

which can be simplified when the second-order infinitesimal quantities are omitted,

$$\delta M < \frac{q_0^2 + \alpha - M_0^2 + 2q_0\delta q}{2M_0}. \quad (36)$$

Now let us analyze the above inequality. For the nonextreme case of the charged 4D EGB black hole, Eq. (36) is never satisfied and thus the cosmic censorship conjecture is maintained because the right-hand side is negative but δM should be positive when the first-order infinitesimal quantity on the numerator is negligible. For the case of the extreme black hole, $M_0^2 = q_0^2 + \alpha$, Eq. (36) reduces to

$$\delta M < \frac{q_0\delta q}{\sqrt{q_0^2 + \alpha}}. \quad (37)$$

Following Ref. [30], we know that the interaction between a static charged BH and a particle gives the relation,

$$\frac{\delta q}{\delta M} = \frac{q_s}{\omega}, \quad (38)$$

and that Eq. (37) reads

$$\omega < \frac{q_0}{\sqrt{q_0^2 + \alpha}} q_s = \Phi_H q_s, \quad (39)$$

where Φ_H is the electric potential at the event horizon. The relationship among reflection, incidence and transmission amplitudes \mathcal{R} , \mathcal{I} and \mathcal{T} of the incident particle is [30]

$$|\mathcal{R}|^2 = |\mathcal{I}|^2 - \frac{\omega - \Phi_H q_s}{\sqrt{\omega^2 - \mu_s^2}} |\mathcal{T}|^2, \quad (40)$$

where μ_s is particle mass. According to Eqs. (39) and (40), $|\mathcal{R}|^2$ is bigger than $|\mathcal{I}|^2$ in the frequency range of Eq. (39), which means that the black hole will emits particles instead of absorbing, known as the superradiation phenomenon, where the mass and charge of the black hole decrease at the same time and the extreme black hole evolves into a sub-extreme configuration. This is contradictory to the precondition that no sub-extreme black holes exist. As a result, the cosmic censorship conjecture guarantees that the singularity can never be naked, which also means that the internal structure behind the event horizon is not able to be observed directly.

2.4 Internal structure of unreachable core regions

We have known from the discussions in subsections 2.1 and 2.2 that Eq. (12) gives the innermost radius that a time-like particle can reach. This means that the geodesic of the particle terminates on the

same sphere surface for both the complex and finite metric functions when the mass and charge are fixed. Using Eqs. (3) and (12) we can check that this radius is less than the inner event horizon, i.e., $r_{\text{in}} < r_{\text{H}}^-$. Thus, the sphere surface with radius r_{in} wraps around a region that is physically unobservable. We can give a close relation between the core region and the metric function: On the surface of the core region the metric function equals one for the three cases — the charged 4D EGB black holes with positive, negative, and vanishing EGB parameters (the case of vanishing EGB parameter corresponds to the RN black hole). In other words, as r_{in} is independent of the EGB parameter α , the core region is same for the metric functions of three cases. Moreover, we notice that the difference of the metric functions is obvious inside but negligible outside the core. For instance, when we take $M = 2.000$ and $|q| = 1.000$, we can see in Fig. 3 that the three metric functions intersect with one point and the differences among the three cases appear apparently inside but not outside the core region.

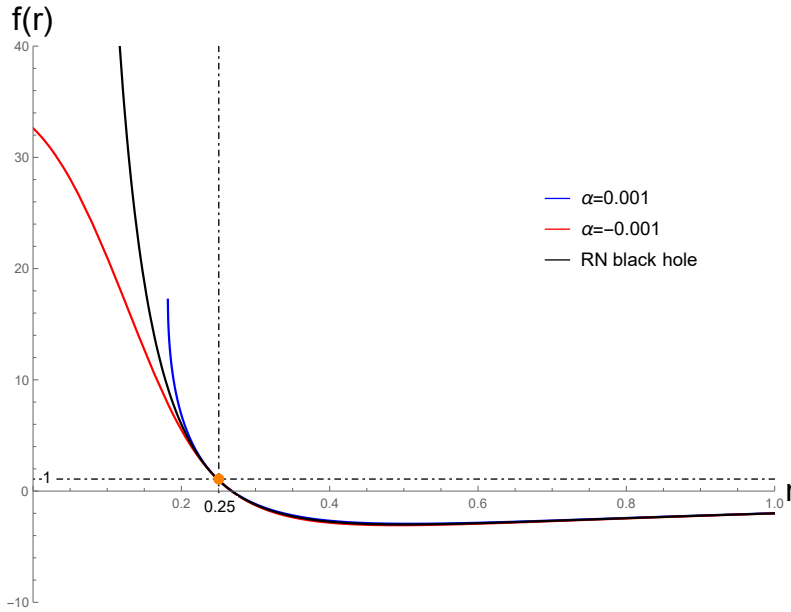


Figure 3: The horizontal axis denotes the radial coordinate and the vertical axis the metric function. The black curve represents the RN black hole, and the blue and red curves represent the charged 4D EGB black hole with the EGB parameters 0.001 and -0.001 , respectively, where the orange dot is the intersection of three curves. Note that the absolute value of the physically allowed α is very small due to $|Q| \equiv |q|/M = 1/2$, see Fig. 2.

Let us make a quantitative analysis of the relative difference between the square of radial velocities of free particles in the charged 4D EGB black hole and that in the RN black hole. The relative difference is

$$\begin{aligned}
 Diff &\equiv \frac{v_{\alpha}^2(r) - v_{\text{RN}}^2(r)}{v_{\text{RN}}^2(r)} = \frac{f_{\text{RN}}(r) - f_{\alpha}(r)}{1 - f_{\text{RN}}(r)} \\
 &= \frac{r^4 + 4\alpha Mr - 2\alpha q^2 - r^2 \sqrt{r^4 + 8\alpha Mr - 4\alpha q^2}}{-4\alpha Mr + 2\alpha q^2}, \tag{41}
 \end{aligned}$$

where v^2 , $f_{\alpha}(r)$, and $f_{\text{RN}}(r)$ are given in Eq. (9), Eq. (1), and Eq. (2), respectively, and the subscripts

α and RN denote the charged 4D EGB black hole and the RN black hole, respectively. For the detailed derivation, see Appendix A. When $r \gg r_{\text{H}}^+$, the absolute value of $Diff$ goes to $|\alpha|M/(2r^3)$, which is very close to zero. We plot Fig. 4 by setting $M = 2.000$ and $|q| = 1.000$, and find that the absolute value of the maximum relative difference of particle velocities is less than 0.030 and this value can be reached only inside the black hole. At the outer horizon of the black hole, $r_{\text{H}}^+ \approx 3.732$, $Diff \approx 0.717 \times 10^{-4}$ if setting $\alpha = -0.001$, and $Diff \approx -0.718 \times 10^{-4}$ if setting $\alpha = 0.001$, and the absolute value of $Diff$ will decrease with the increasing of the radial distance. Consequently, it is not realistic to distinguish the internal structures of three black holes (the charged 4D EGB black holes with positive and negative EGB parameters and the RN black hole) by the difference of particle motion. We thus turn to the thermodynamic and dynamic behaviors of three black holes that will represent the different internal structures of black holes.

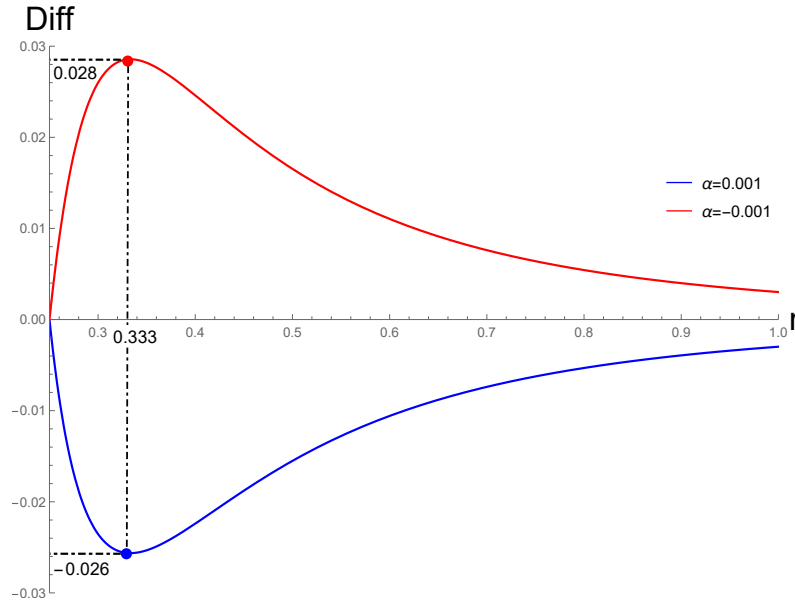


Figure 4: The horizontal axis denotes the radial coordinate and the vertical axis the relative difference of particle velocities. The blue and red curves represent the charged 4D EGB black hole with the EGB parameters 0.001 and -0.001 , respectively.

3 Second-order phase transition

Now we discuss the behaviors of Davies points associated with second-order phase transitions in the charged 4D EGB black hole.

The Davies points can be obtained from the solutions of the algebraic equation, $1/C_{q,\alpha} = 0$, where $C_{q,\alpha}$, the heat capacity with a fixed q and α , is divergent at the Davies points. Here we write this heat capacity in its dimensionless form,

$$C_{q,\alpha}/M^2 \equiv \frac{1}{M^2} \left(\frac{\partial M}{\partial T} \right)_{q,\alpha} = \frac{4\pi x_{\text{H}}^+(x_{\text{H}}^+ - 1)(x_{\text{H}}^{+2} + 2a)^2}{-x_{\text{H}}^{+4} + (3x_{\text{H}}^{+2} + 2a)Q^2 + 5x_{\text{H}}^{+2}a + 2a^2}, \quad (42)$$

and then obtain the master equation that determines the Davies points,

$$-x_{\text{H}}^{+4} + (3x_{\text{H}}^{+2} + 2a)Q^2 + 5x_{\text{H}}^{+2}a + 2a^2 = 0,$$

where Q and a are dimensionless charge and EGB parameter, respectively, see Eq. (22). The above equation can be expressed in terms of Q and a when the dimensionless event horizon x_{H}^+ , Eq. (26), is substituted,

$$(4 - 5Q^2 - 7a)\sqrt{1 - Q^2 - a} - (7 - 2Q^2 - 4a)Q^2 + 2a^2 - 9a - 4 = 0. \quad (43)$$

3.1 Phase transition associated with the complex metric function

For the case of the positive EGB parameter, $\alpha > 0$ or $a > 0$, we plot the $|Q| - a$ graph in Fig. 5 showing the curve of Davies points together with the curves of the physical bound and the evolution with respect to mass.

The physically allowed region of Q and a is determined by the fact that the charged 4D EGB black hole must have an event horizon, see Eq. (4), which, together with Eq. (22), gives the inequality, $1 - Q^2 - a \geq 0$. That is, the physically allowed region (in gray color) is surrounded by the red curve,⁴ $a = 1 - Q^2$, the horizontal axis, and the vertical axis for the case of $a > 0$. The blue curve corresponds to the Davies points and is determined by Eq. (43).

There are three parameters, M , q , and α , that depict this black hole, and the evolution can be analyzed in principle with respect to any one of them. Considering the achievement that the Davies points have been calculated under a fixed q and α , see Eqs. (42) and (43), we thus investigate the evolution correspondingly by fixing the two parameters but varying the mass. Moreover, based on the definitions of the dimensionless parameters Q and a , see Eq. (22), we obtain the following relation,

$$\frac{a}{Q^2} = \frac{\alpha}{q^2} = \text{const.} \equiv C, \quad (44)$$

which gives the cluster of evolution curves,

$$a = CQ^2, \quad (45)$$

where C is the coefficient for a fixed q and α on the $|Q| - a$ plane. Because α is positive and $|q|$ can be very small or large, C can take any positive value in principle, i.e., $C \in (0, \infty)$. The cluster of evolution curves describes the black hole evolution with respect to mass M . As the heat capacity is calculated by fixing α and q , C is constant for a fixed Davies point. Obviously, this cluster of evolution curves is quadratic and passes through the origin of the $|Q| - a$ plane. For instance, we take $C = 1.000, 2.000, 3.000$, which corresponds to the magenta, green, and yellow curves, respectively, in Fig. 5. In general, this cluster of evolution curves looks similar for any positive C . This implies that the charged 4D EGB black hole will no doubt pass through one Davies point during its evolution. In other words, one second-order phase transition must happen when the black hole evolves with respect to mass.

⁴It has the same formula as Eq. (30) associated with the negative EGB parameter because the existence of horizons is same for the both cases of the positive and negative EGB parameters, see Eq. (4.)

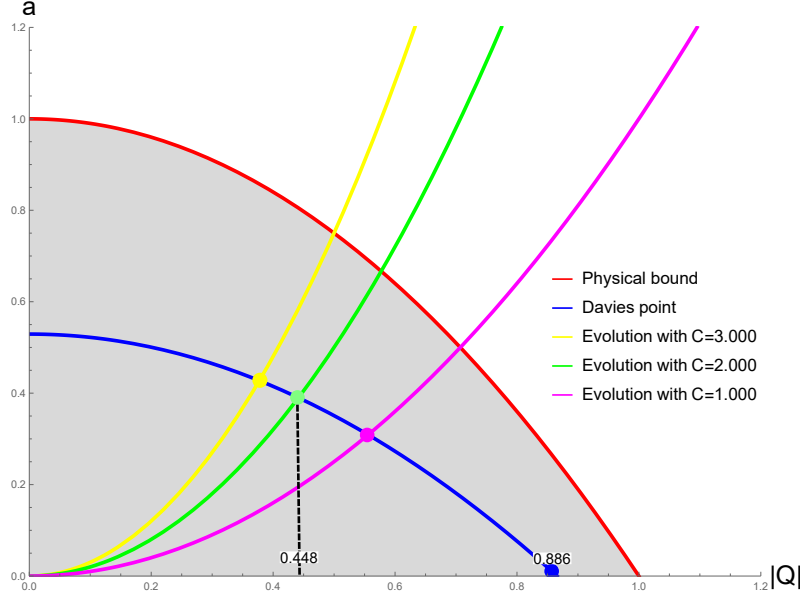


Figure 5: The behaviors of Davies points are shown on the $|Q| - a$ plane when the EGB parameter is positive for the charged 4D EGB black hole. The horizontal axis denotes the absolute value of the rescaled charge, and the vertical axis the rescaled EGB parameter. The red curve determines the boundary of the physically allowed region (in gray color) and the blue curve corresponds to the Davies points. The magenta, green, and yellow curves correspond to the evolution of the black hole with respect to mass when we take $C = 1.000, 2.000, 3.000$, respectively.

We note that the Davies point of the RN black hole is located at the intersection of the blue curve and the horizontal axis, corresponding to the case of $a = 0$, see the blue dot in Fig. 5. Moreover, the charge mass ratio, $\frac{|q|}{M}$, i.e. the absolute value of the rescaled charge $|Q|$ of the charged 4D EGB black hole at the Davies points is always smaller than that of the RN black hole. This consequence is obvious when we compare the Davies point of the charged 4D EGB black hole (intersection of the blue and magenta curves, or that of the blue and green curves, or that of the blue and yellow curves) with the Davies point of the RN black hole (intersection of the blue curve and the horizontal axis).

3.2 Phase transition associated with the finite metric function

Now we turn to the case of the negative EGB parameter, $\alpha < 0$ or $a < 0$. Based on Fig. 2, we plot the $|Q| - a$ graph in Fig. 6 showing the curve of Davies points together with the curves of the physical bound and the evolution with respect to mass. The red and brown curves are governed by Eq. (30) and Eq. (31), respectively, see the explanation below Eq. (31). They determine the physical region (in gray color) in which the charged 4D EGB black hole with the finite metric function must have a horizon. The blue curve indicating the Davies points is still governed by Eq. (43), and the cluster of evolution curves by Eq. (45), where the former is related to a negative a and the latter to a negative C .

The brown and blue curves intersect at one point: $(|Q|, a) = (0.956, -0.113)$, and the red, brown and blue curves intersect at the end of the three curves : $(|Q|, a) = (\sqrt{\frac{3}{2}}, -\frac{1}{2})$, where a takes its minimum.

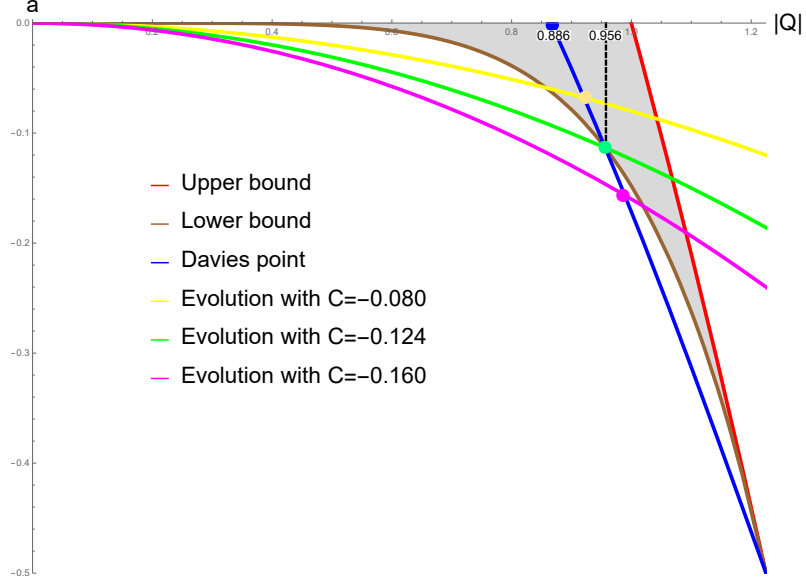


Figure 6: The behaviors of Davies points are shown on the $|Q| - a$ plane when the EGB parameter is negative for the charged 4D EGB black hole. The horizontal axis denotes the absolute value of the rescaled charge, and the vertical axis the rescaled EGB parameter. The red and brown curves determine the upper and lower boundaries of the physically allowed region (in gray color), respectively. The blue curve corresponds to the Davies points. The magenta, green, and yellow curves correspond to the evolution of the black hole with respect to mass when we take $C = -0.160, -0.124, -0.080$, respectively. The brown, blue and green curves intersect at the point: $(0.956, -0.113)$.

The intersection of the brown and blue curves in Fig. 6 can be solved from the combination of their formulas, Eq. (31) and Eq. (43), and then the specific coefficient can be computed by its definition, Eq. (44), $C = -\frac{0.113}{0.956^2} = -0.124$. As a result, we can determine the formula governing the green curve, $a = -0.124Q^2$. We can see that only the interval of the blue curve between $(|Q|, a) = (0.886, 0)$ and $(|Q|, a) = (0.956, -0.113)$ is located inside the physical region (in gray color), i.e., only the Davies points on this interval are allowed physically, where the physical permission means the existence of horizons for the 4D EGB black hole.

In Fig. 6 the range of C is $C \in (-\frac{1}{3}, 0)$, where the intersection of the red, brown and blue curves, $(|Q|, a) = (\sqrt{\frac{3}{2}}, -\frac{1}{2})$, gives the end point of the three curves, see Eq. (44). The green dot divides the blue curve representing the Davies points into two parts, with the upper part, $C \in [-0.124, 0)$, located inside the physical region and the lower part, $C \in (-\frac{1}{3}, -0.124)$, outside the physical region. If the cluster of evolution curves, i.e. $a = CQ^2$, goes through the upper part of the blue curve and intersects with the blue one, e.g. the yellow curve, the intersection is located inside the physical region; if it goes through the lower part of the blue curve and intersects with the blue one, e.g. the magenta curve, the intersection is located outside the physical region. Therefore, the black holes associated with $C \in [-0.124, 0)$ will undergo a phase transition during the evolution, but those associated with $C \in (-\frac{1}{3}, -0.124)$ will not. We can say, the green dot associated with $C = -0.124$ is the split point of whether the black hole has a phase transition or not.

It is worth mentioning the end point, $(|Q|, a) = (\sqrt{\frac{3}{2}}, -\frac{1}{2})$, which corresponds to the coefficient $C = -\frac{1}{3}$. As discussed in subsection 2.2, the charged 4D EGB black hole at this point stays in its extreme configuration with only one horizon. From Fig. 6, we can see that the end point is a Davies point, but the black hole in the extreme configuration cannot evolve to the other non-extreme configurations. For the same reason, the other non-extreme configurations cannot evolve to the extreme configuration, either. This consequence is obvious because the blue curve between $(|Q|, a) = (0.956, -0.113)$ and $(|Q|, a) = (\sqrt{\frac{3}{2}}, -\frac{1}{2})$, i.e., $C \in (-\frac{1}{3}, -0.124)$, is beyond the physical region.

Let us make a comparison between the case of the positive EGB parameter (depicted by Fig. 5) and the case of the negative EGB parameter (depicted by Fig. 6). For the former, we can see in Fig. 5 that the whole blue curve is located inside the physical region (in gray color) and that the cluster of evolution curves, $a = CQ^2$, $C \in (0, \infty)$, intersects with the blue one for any positive C . In other words, all the Davies points are allowed physically. For the latter, we can see in Fig. 6 that only the upper part between $(|Q|, a) = (0.886, 0)$ and $(|Q|, a) = (0.956, -0.113)$ is located inside the physical region (in gray color) and that the cluster of evolution curves, $a = CQ^2$, intersects with the blue one in the physical region when $C \in [-0.124, 0)$. In other words, only one part of the Davies points is allowed physically. This is the crucial difference between the two cases. In addition, the charge mass ratio $\frac{|q|}{M}$ of the charged 4D EGB black hole at the Davies points of the physical region is always smaller than that of the RN black hole for the former case (Fig. 5), but it is always larger than that of the RN black hole for the latter case (Fig. 6).

3.3 Heat capacity and temperature at a Davies point associated with the complex and finite metric functions

Let us discuss the behaviors of the heat capacity and temperature when a charged 4D EGB black hole evolves through a Davies point. Based on the definition of the heat capacity with a fixed q and α , Eq. (42), we derive the temperature during the evolution,

$$T = \int_{\ell} dT = \int_{\ell} \left(\frac{\partial T}{\partial M} \right)_{q, \alpha} dM = \int_{\ell} \frac{dM}{C_{q, \alpha}}, \quad (46)$$

where “ ℓ ” means the evolutionary path of charged 4D EGB black holes. We can conclude that a Davies point corresponds to a saddle point of the curve of temperature versus mass. As to whether the saddle point corresponds to a maximum or a minimum, we have to analyze by considering a positive EGB parameter and a negative one separately.

At first, we examine the relationship between the heat capacity and mass of the black hole when $\alpha > 0$ or $a > 0$. We plot the $M - C_{q, \alpha}$ graph in Fig. 7 by using Eq. (42) and Eq. (26) and replacing Q and a by M , q , and α . For each of $\alpha = 0.100, 0.200, \dots, 0.500$ with the fixed $q = 1.000$, we can see that the heat capacity changes from positive to negative when the black hole mass increases and passes through the corresponding Davies point, indicating that this Davies point is the only saddle point with the maximal temperature.

Then we turn to investigate the relationship between the heat capacity and mass when $\alpha < 0$ or $a < 0$, and classify this case into two subcases which correspond to $-0.124 \leq \frac{\alpha}{q^2} < 0$ and $-\frac{1}{3} < \frac{\alpha}{q^2} < -0.124$,

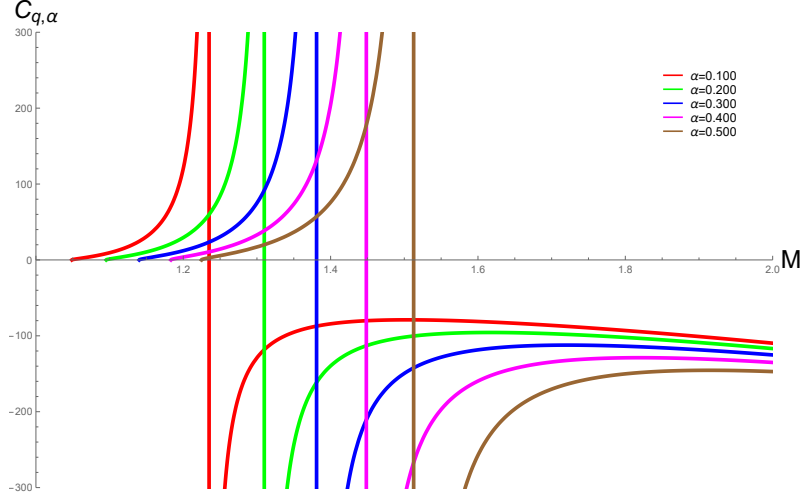


Figure 7: The relationship between the heat capacity and mass when the EGB parameter is positive for the charged 4D EGB black hole. The EGB parameter α is set to be $\alpha = 0.100, 0.200, \dots, 0.500$, and the charge $q = 1.000$. One vertical line corresponds to one Davies point for each value of α .

respectively. As done in the above case, we plot the $M - C_{q,\alpha}$ graphs in Fig. 8 when α is set to be $-0.100, -0.090, \dots, -0.060$ and $q = 1.000$ for the first subcase, and in Fig. 9 when α is set to be $-0.170, -0.160, \dots, -0.130$ and $q = 1.000$ for the second subcase. From Fig. 8, we can see that the Davies points exist in the process of evolution of the black hole, and that the heat capacity still goes from positive to negative when the mass increases and passes through the corresponding Davies point, indicating that this Davies point is the only saddle point with the maximal temperature. From Fig. 9, we can see, however, that the black hole does not pass through any Davies points during its evolution, and that the temperature increases monotonously with the increasing of mass. Note that for the extreme configuration, $\frac{\alpha}{q^2} = -\frac{1}{3}$, it is isolated by the evolution although it is a Davies point as explained in subsection 3.2.

4 Quasinormal modes in the eikonal limit

According to the light ring/quasinormal mode correspondence [24], the quasinormal mode frequencies of a test scalar fields perturbation in the eikonal limit are of the following form for a static and spherically symmetric black hole,

$$\omega = \Omega_c l - i(n + 1/2)|\lambda|, \quad (47)$$

where the angular velocity Ω_c and the Lyapunov index λ can be computed by

$$\Omega_c = \frac{\sqrt{f_c}}{r_c}, \quad \lambda = \sqrt{\frac{f_c(2f_c - r_c^2 f_c'')}{2r_c^2}}. \quad (48)$$

Here l is the multiple number, where the eikonal limit means $l \gg 1$; n is the overtone number; $f_c \equiv f(r_c)$ and $f_c'' \equiv f''(r)|_{r=r_c}$, where the prime means the derivative with respect to r and r_c , the radius of a photon

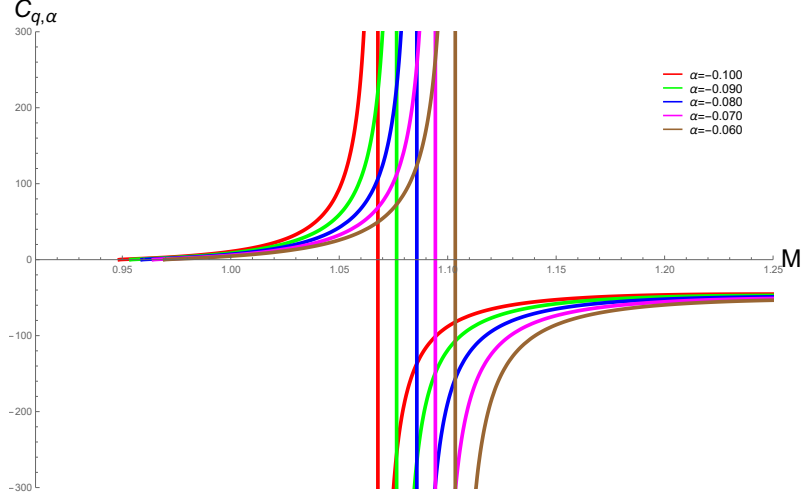


Figure 8: The relationship between the heat capacity and mass when the EGB parameter is negative and located in the range of $-\frac{1}{3} < \frac{\alpha}{q^2} < 0$ for the charged 4D EGB black hole. The EGB parameter α is set to be $\alpha = -0.100, -0.090, \dots, -0.060$, and the charge $q = 1.000$. One vertical line corresponds to one Davies point for each value of α .

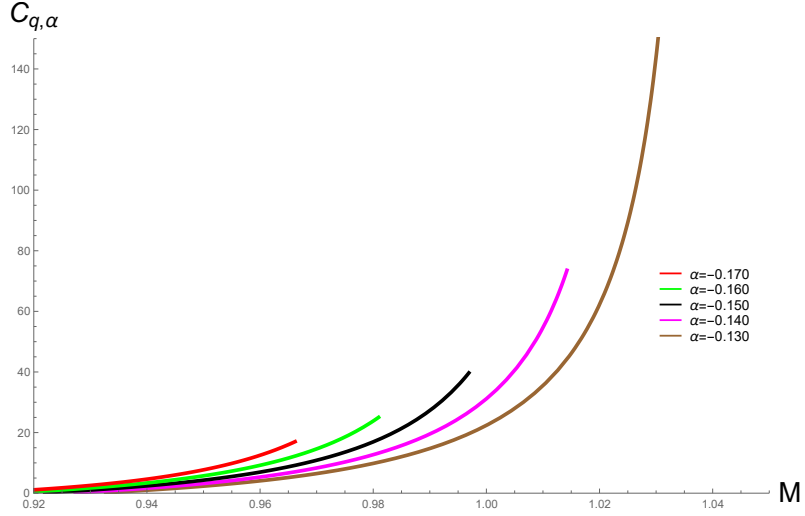


Figure 9: The relationship between the heat capacity and mass when the EGB parameter is negative and located in the range of $-\frac{1}{3} < \frac{\alpha}{q^2} < -0.124$ for the charged 4D EGB black hole. The EGB parameter α is set to be $\alpha = -0.170, -0.160, \dots, -0.130$, and the charge $q = 1.000$. The black hole does not pass through any Davies points during its evolution and its temperature increases monotonously with the increasing of mass.

sphere, satisfies the following equation,

$$2f(r_c) - rf'(r_c) = 0. \quad (49)$$

When substituting the shape function Eq. (1) of the charged 4D EGB black hole into Eq. (49), we

obtain the relationship between r_c and the three parameters of this black hole,

$$r_c^4 - 9M^2 r_c^2 + 4M(3q^2 + \alpha)r_c - 4q^2(q^2 + \alpha) = 0, \quad (50)$$

and we also derive the angular velocity Ω_c and the Lyapunov index λ by substituting Eq. (1) into Eq. (48),

$$\Omega_c^2 = \frac{f_c}{r_c^2} = \frac{1}{r_c^2} + \frac{1 - A^{1/2}(r_c)}{2\alpha}, \quad (51a)$$

$$\lambda^2 = \frac{f_c(2f_c - r_c^2 f_c'')}{2r_c^2} = \frac{f(r_c)}{r_c^8 A^{3/2}(r_c)} \left(r_c^6 A^{3/2}(r_c) - 2r_c^4 q^2 - 36r_c^2 M^2 \alpha + 32r_c M q^2 \alpha - 8q^4 \alpha \right), \quad (51b)$$

where

$$A(r_c) \equiv 1 + 4\alpha \left(\frac{2M}{r_c^3} - \frac{q^2}{r_c^4} \right). \quad (52)$$

By using the rescaled quantities, Q , a , and x_c , see Eqs. (22) and (25), we can rewrite the above relations in a dimensionless form,

$$x_c^4 - 9x_c^2 + 4(3Q^2 + a)x_c - 4Q^2(Q^2 + a) = 0, \quad (53)$$

$$\Omega_c^2 M^2 = \frac{1}{x_c^2} + \frac{1 - A^{1/2}(x_c)}{2a}, \quad (54)$$

$$\lambda^2 M^2 = \frac{f(x_c)}{x_c^8 A^{3/2}(x_c)} \left(x_c^6 A^{3/2}(x_c) - 2x_c^4 Q^2 - 36x_c^2 a + 32x_c Q^2 a - 8Q^4 a \right), \quad (55)$$

where $f(x_c)$ and $A(x_c)$ are defined by

$$f(x_c) \equiv 1 + \frac{x_c^2}{2a} \left[1 - \sqrt{1 + 4a \left(\frac{2}{x_c^3} - \frac{Q^2}{x_c^4} \right)} \right], \quad (56)$$

$$A(x_c) \equiv 1 + 4a \left(\frac{2}{x_c^3} - \frac{Q^2}{x_c^4} \right). \quad (57)$$

4.1 Quasinormal modes in the eikonal limit associated with the complex metric function

Now we plot the $\Omega_c M - \lambda M$ graph for the positive EGB parameter ($\alpha > 0$ or $a > 0$) in Fig. 10 in terms of Eqs. (53)-(57), where the parameter is set to be $a = 0.100, 0.200, \dots, 0.900$, and $a = 0$ corresponding to the RN black hole is attached for comparison. Note that the range of Q that is physically allowed in the figure depends on the range of a , that is, the ranges of Q and a should ensure the existence of a horizon, i.e., to satisfy Eq. (26).

We can see from Fig. 10 that the ranges of the angular velocity for different values of the parameter a are restricted within the range of the angular velocity of the RN black hole. For instance, see the red curve ($a = 0.100$), its range of the horizontal coordinate is completely covered by the range of the horizontal coordinate of the black curve ($a = 0$). In other words, we cannot distinguish the 4D EGB black hole from the RN black hole when we observe the angular velocity only. Note that the angular

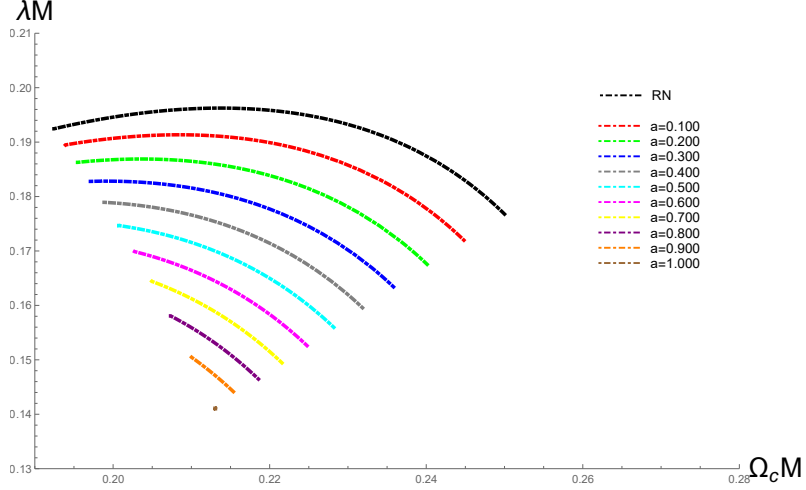


Figure 10: The relationship between the angular velocity and Lyapunov index for the positive EGB parameter. The horizontal axis denotes the dimensionless angular velocity, and the vertical one the dimensionless Lyapunov index. The black curve corresponds to the RN black hole and the other curves correspond to the charged 4D EGB black hole with different values of the positive EGB parameter.

velocity of the photon sphere corresponds to the oscillating frequency in quasinormal modes. That is to say, we cannot distinguish the charged 4D EGB black hole from the RN black hole just by means of the oscillating frequency of quasinormal modes. Fortunately, the range of the Lyapunov index for the charged 4D EGB black hole cannot be covered completely by that of the RN black hole. For instance, the minimum value of λM in the 4D EGB black hole is 0.141 which appears when $a = 1.000$ and $Q = 0$,⁵ while the range of λM in the RN black hole is $0.177 \leq \lambda M \leq 0.196$. This implies that the Lyapunov index of the charged 4D EGB black hole can be smaller than the minimum Lyapunov index of the RN black hole. Therefore, we have the possibility to distinguish the charged 4D EGB black hole from the RN black hole when we observe the Lyapunov index.

It is known that the imaginary part of quasinormal mode frequencies is inversely proportional to the damping time of a test scalar field perturbation,

$$\tau \propto \frac{1}{|\omega_I|}, \quad (58)$$

which means the time past for the amplitude of a test scalar field perturbation to decay to e^{-1} of its original value. Thus, the damping time of the uncharged 4D EGB black hole will be longer than the maximum damping time of the RN black hole if a is appropriately chosen,⁶ and the maximum relative deviation between the damping time of 4D EGB black holes and that of the RN black hole equals

$$\frac{\Delta\tau_1}{\tau_1} = \frac{\frac{1}{0.141} - \frac{1}{0.177}}{\frac{1}{0.177}} \approx 25.5\%. \quad (59)$$

⁵When a is taken to be one, Q must be zero in order to ensure the existence of a horizon. That is, the charged 4D EGB black hole becomes its uncharged case if $a = 1.000$, see Eq. (26).

⁶This consequence is also valid for the charged 4D EGB black hole if Q and a are appropriately chosen in accordance with Eq. (26).

4.2 Quasinormal modes in the eikonal limit and shadow radii associated with the finite metric function

Now we plot the $\Omega_c M - \lambda M$ graph for the negative EGB parameter ($\alpha < 0$ or $a < 0$) in Fig. 11 in terms of Eqs. (53)-(57), where the parameter is set to be $a = -0.050, -0.100, \dots, -0.450$, and $a = 0$ corresponding to the RN black hole is attached for comparison. Note that the range of Q that is physically allowed in the figure depends on the range of a , that is, the ranges of Q and a should coincide with the constraints Eqs. (23a), (23b), and (29), i.e., they have to be located in the physical region depicted in Fig. 2.

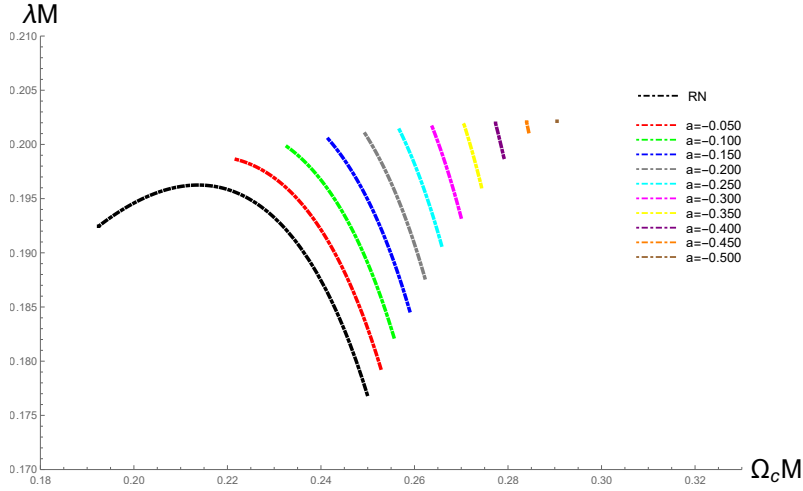


Figure 11: The relationship between the angular velocity and Lyapunov index for the negative EGB parameter. The horizontal axis denotes the dimensionless angular velocity, and the vertical one the dimensionless Lyapunov index. The black curve corresponds to the RN black hole and the other curves correspond to the charged 4D EGB black hole with different values of the negative EGB parameter.

We can see from Fig. 11 that both the range of the angular velocity and that of the Lyapunov index for the charged 4D EGB black hole cannot be covered completely by those of the RN black hole. For the angular velocity, the maximum value of $\Omega_c M$ for the charged 4D EGB black hole is 0.291 at $a = -0.500$, while the range for the RN black hole is $0.192 \leq \Omega_c M \leq 0.250$. This means that the angular velocity of the 4D EGB black hole is larger than the maximum value of the RN black hole. Therefore, we have the possibility to distinguish the two types of black holes when we observe the angular velocity. For the Lyapunov exponent, the maximum value of the charged 4D EGB black hole can be up to 0.202 when $a = -0.500$, while the range of λM for the RN black hole is $0.177 \leq \lambda M \leq 0.196$. This implies that the Lyapunov exponent of the charged 4D EGB black hole is larger than the maximum of the RN black hole, which suggests that we can also have the possibility to distinguish the two types of black holes when we observe the Lyapunov exponent.

As a result, the damping time of the charged 4D EGB black hole can be shorter than the minimum damping time of the RN black hole, and the maximum relative deviation between them is

$$\frac{\Delta\tau_2}{\tau_2} = \frac{\frac{1}{0.202} - \frac{1}{0.196}}{\frac{1}{0.196}} \approx -3.0\%, \quad (60)$$

where the minus sign means that the damping time of the charged 4D EGB black hole is smaller than the minimum damping time of the RN black hole. Moreover, the oscillating frequency of the charged 4D EGB black hole can be higher than the maximum oscillating frequency of the RN black hole, and the maximum relative deviation between them is

$$\frac{\Delta\omega_{R2}}{\omega_{R2}} = \frac{0.291 - 0.250}{0.250} = 16.4\%. \quad (61)$$

Alternatively, we may distinguish the charged 4D EGB black hole from the RN black hole by using their shadow radii. The shadow radius R_{sh} observed at infinity outside a black hole is closely related [26] to the angular velocity of the photon sphere,

$$R_{\text{sh}} = \frac{r_c}{\sqrt{f(r_c)}} = \Omega_c^{-1}. \quad (62)$$

Therefore, the shadow radius of the charged 4D EGB black hole can be smaller than the minimum shadow radius of the RN black hole when the EGB parameter is negative, and the maximum relative deviation between them is

$$\frac{\Delta R_{\text{sh}}}{R_{\text{sh}}} = \frac{\frac{1}{0.291} - \frac{1}{0.250}}{\frac{1}{0.250}} \approx -14.1\%, \quad (63)$$

where the minus sign has the similar meaning to that mentioned above. As a result, the shadow radius of the charged 4D EGB black hole is smaller than the smallest shadow radius of the RN black hole in the case of the finite metric function, which does not happen in the case of the complex metric function.

Comparing the case of the complex metric function (positive EGB parameter) with the case of the finite metric function (negative EGB parameter), we find their dynamic difference in the angular velocity and Lyapunov exponent or in the oscillating frequency and damping time. This may give the possibility to shed some light on the interior of black holes (depicted partially by metric functions) from the exterior (shown partially by dynamic properties).

5 Conclusion

In this paper, our main work is to connect an undetectable property of black holes — the metric singularity at a black hole center to a probably observable phenomenon or variable, such as the second-order phase transition of black holes, the oscillating frequency and damping time of perturbation of a test scalar field, and the shadow radius of black holes. For the charged 4D EGB black hole, if the EGB parameter is positive, the metric is singular at the center; if the EGB parameter is negative and located in the physically allowed region shown in Fig. 2, the metric is non-singular. We try to distinguish the charged 4D EGB black hole with or without the metric function singularity from the Reissner-Nordström black hole by investigating the behaviors of the Davies point and calculating the quasinormal modes in the eikonal limit. We summarize the following differences between the characteristic variables of thermodynamics and dynamics in the charged 4D EGB black hole and the same variables in the Reissner-Nordström black hole.

- When the EGB parameter is positive or negative in the range of $-0.124 \leq \frac{\alpha}{q^2} < 0$, the charged 4D EGB black hole will pass through one Davies point in the evolution with respect to mass, which indicates that there exists one unique saddle point with the maximum temperature. However, if the EGB parameter is negative in the range of $-\frac{1}{3} < \frac{\alpha}{q^2} < -0.124$, the black hole will not pass through a Davies point in the evolution and its temperature will not have an extremum, either. Compared with the second-order phase transition point of the RN black hole, the charge mass ratio $\frac{|q|}{M}$ at the Davies point is smaller than that of the RN black hole for the positive EGB parameter, while it is larger than that of the RN black hole for the negative EGB parameter of the range $-0.124 \leq \frac{\alpha}{q^2} < 0$.
- When the EGB parameter is positive, the oscillating frequency of quasinormal modes of a test scalar field perturbation in the eikonal limit will not exceed the range of oscillating frequencies of the RN black hole, but the damping time can be longer than the maximum damping time of the RN black hole. When the EGB parameter is negative, the oscillating frequency can be higher than the maximum oscillating frequency of the RN black hole and the damping time shorter than the minimum damping time of the RN black hole.
- When the EGB parameter is positive, the charged 4D EGB black hole cannot be distinguished from the RN black hole by means of a shadow radius. Nonetheless, the shadow radius of the charged 4D EGB black hole will be smaller than the minimum shadow radius of the RN black hole when the EGB parameter is negative.

Acknowledgments

The authors would like to thank X.-C. Cai, C. Lan, and Y.C. Ong for useful discussions. This work was supported in part by the National Natural Science Foundation of China under grant Nos. 11675081 and 12175108. The authors would like to thank the anonymous referee for the helpful comments that improve this work greatly.

Appendix

A Derivation of the relative difference

The derivation is based on *Mathematical Theory of Black Holes* by Chandrasekhar [27].

For a general spherically symmetric spacetime, the Lagrangian of a free neutral particle is

$$\mathcal{L} = \frac{1}{2} \left\{ -f(r)\dot{t}^2 + [f(r)]^{-1}\dot{r}^2 + r^2\dot{\theta}^2 + (r^2 \sin^2 \theta)\dot{\phi}^2 \right\}, \quad (\text{A.1})$$

where the dot represents the derivative with respect to the affine parameter τ . The corresponding canon-

ical momenta read

$$\begin{aligned} p_t &:= -\frac{\partial \mathcal{L}}{\partial \dot{t}} = f(r)\dot{t}, & p_r &:= \frac{\partial \mathcal{L}}{\partial \dot{r}} = [f(r)]^{-1}\dot{r}, \\ p_\theta &:= \frac{\partial \mathcal{L}}{\partial \dot{\theta}} = r^2\dot{\theta}, & p_\phi &:= \frac{\partial \mathcal{L}}{\partial \dot{\phi}} = r^2\dot{\phi} \sin^2 \theta. \end{aligned} \quad (\text{A.2})$$

The resulting Hamiltonian takes the form,

$$\mathcal{H} = -p_t \dot{t} + (p_r \dot{r} + p_\theta \dot{\theta} + p_\phi \dot{\phi}) - \mathcal{L} = \mathcal{L}. \quad (\text{A.3})$$

The constancy of the Hamiltonian gives rise to

$$\mathcal{H} = \mathcal{L} = \text{const}. \quad (\text{A.4})$$

By rescaling the affine parameter τ , we can take this constant to be $-\frac{1}{2}, 0, \frac{1}{2}$, corresponding to the time-like, null, and space-like cases, respectively. Moreover, the Hamiltonian canonical equations lead to the following integrals of motion,

$$\frac{dp_t}{d\tau} = \frac{\partial \mathcal{L}}{\partial t} = 0, \quad \frac{dp_\phi}{d\tau} = -\frac{\partial \mathcal{L}}{\partial \phi} = 0. \quad (\text{A.5})$$

Considering the motion of a particle on the equatorial plane, $\theta = \pi/2$, we can define the energy per unit mass E and angular momentum L as

$$p_t = \text{const.} \equiv E, \quad p_\phi = r^2 \frac{d\phi}{d\tau} = \text{const.} \equiv L, \quad p_\theta = r^2 \dot{\theta} = 0. \quad (\text{A.6})$$

So the Lagrangian of the particle can be written as

$$2\mathcal{L} = -\frac{E^2}{f(r)} + \frac{\dot{r}^2}{f(r)} + \frac{L^2}{r^2} = -1. \quad (\text{A.7})$$

For free particles in the radial motion, we know $L = 0$ and $E^2 = 1$. Thus, the square of velocity associated with τ of a free neutral particle is

$$v^2 = \left(\frac{dr}{d\tau} \right)^2 = 1 - f(r). \quad (\text{A.8})$$

According to the definition of the relative difference, we obtain

$$\text{Diff} \equiv \frac{v_\alpha^2(r) - v_{\text{RN}}^2(r)}{v_{\text{RN}}^2(r)} = \frac{f_{\text{RN}}(r) - f_\alpha(r)}{1 - f_{\text{RN}}(r)}, \quad (\text{A.9})$$

which is just Eq. (41) when $f_\alpha(r)$ (Eq. (1)) and $f_{\text{RN}}(r)$ (Eq. (2)) are considered.

References

- [1] D. Lovelock, *The Einstein tensor and its generalizations*, J. Math. Phys. **12** (1971) 498;
D. Lovelock, *The four-dimensionality of space and the Einstein tensor*, J. Math. Phys. **13** (1972) 874;
C. Lanczos, *A remarkable property of the Riemann-Christoffel tensor in four dimensions*, Ann. Math. (N.Y.) **39** (1938) 842.
- [2] R.-G. Cai, L.-M. Cao, and N. Ohta, *Black holes in gravity with conformal anomaly and logarithmic term in black hole entropy*, J. High Energy Phys. **04** (2010) 082; [arXiv:0911.4379 [hep-th]]
R.-G. Cai, *Thermodynamics of conformal anomaly corrected black holes in AdS space*, Phys. Lett. **B 733** (2014) 183. [arXiv:1405.1246 [hep-th]]
- [3] G. Cognola, R. Myrzakulov, L. Sebastiani, and S. Zerbini, *Einstein gravity with Gauss-Bonnet entropic corrections*, Phys. Rev. **D 88** (2013) 024006. [arXiv:1304.1878 [gr-qc]]
- [4] D. Glavan and C. Lin, *Einstein-Gauss-Bonnet gravity in four-dimensional spacetime*, Phys. Rev. Lett. **124** (2020) 081301. [arXiv:1905.03601 [gr-qc]]
- [5] P.G.S. Fernandes, *Charged black holes in AdS spaces in 4D Einstein Gauss-Bonnet gravity*, Phys. Lett. **B 805** (2020) 135468. [arXiv:2003.05491 [gr-qc]]
- [6] A. Kumar and R. Kumar, *Bardeen black holes in the novel 4D Einstein-Gauss-Bonnet gravity*, arXiv:2003.13104 [gr-qc].
- [7] S.G. Ghosh and S.D. Maharaj, *Noncommutative inspired black holes in regularised 4D Einstein-Gauss-Bonnet theory*, Phys. Dark Univ. **31** (2021) 100793. [arXiv:2004.13519 [gr-qc]]
- [8] K. Yang, B.-M. Gu, S.-W. Wei, and Y.-X. Liu, *Born-Infeld black holes in novel 4D Einstein-Gauss-Bonnet gravity*, Eur. Phys. J. **C 80** (2020) 662. [arXiv:2004.14468 [gr-qc]]
- [9] M. Gurses, T.C. Sisman, and B. Tekin, *Is there a novel Einstein-Gauss-Bonnet theory in four dimensions?*, Eur. Phys. J. **C 80** (2020) 647. [arXiv:2004.03390 [gr-qc]]
- [10] F.-W. Shu, *Vacua in novel 4D Einstein-Gauss-Bonnet gravity: Pathology and instability?*, Phys. Lett. **B 811** (2020) 135907. [arXiv:2004.09339 [gr-qc]].
- [11] W.-Y. Ai, *A note on the novel 4D Einstein-Gauss-Bonnet gravity*, Commun. Theor. Phys. **72** (2020) 095402; [arXiv:2004.02858 [gr-qc]]
S. Mahapatra, *A note on the total action of 4D Gauss-Bonnet theory*, Eur. Phys. J. **C 80** (2020) 992; [arXiv:2004.09214 [gr-qc]]
R.A. Hennigar, D. Kubiznak, R.B. Mann, and C. Pollack, *On taking the $D \rightarrow 4$ limit of Gauss-Bonnet gravity: Theory and solutions*, J. High Energy Phys. **07** (2020) 027; [arXiv:2004.09472 [gr-qc]]

- J. Arrechea, A. Delhom, and A. Jiménez-Cano, *Yet another comment on four-dimensional Einstein-Gauss-Bonnet gravity*, Chin. Phys. **C 45** (2021) 013107. [arXiv:2004.12998 [gr-qc]]
- [12] H. Lü and Y. Pang, *Horndeski gravity as $D \rightarrow 4$ limit of Gauss-Bonnet*, Phys. Lett. **B 809** (2020) 135717; [arXiv:2003.11552 [gr-qc]]
T. Kobayashi, *Effective scalar-tensor description of regularized Lovelock gravity in four dimensions*, J. Cosmo. Astropart. Phys. **07** (2020) 013; [arXiv:2003.12771 [gr-qc]]
P.G.S. Fernandes, P. Carrilho, T. Clifton, and D.J. Mulryne, *Derivation of regularized field equations for the Einstein-Gauss-Bonnet theory in four dimensions*, Phys. Rev. **D 102** (2020) 024025. [arXiv:2004.08362 [gr-qc]]
- [13] K. Aoki, M.A. Gorji, and S. Mukohyama, *A consistent theory of $D \rightarrow 4$ Einstein-Gauss-Bonnet gravity*, Phys. Lett. **B 810** (2020) 135843. [arXiv:2005.03859 [gr-qc]]
- [14] M. Guo and P.-C. Li, *The innermost stable circular orbit and shadow in the novel 4D Einstein-Gauss-Bonnet gravity*, Eur. Phys. J. **C 80** (2020) 588; [arXiv:2003.02523 [gr-qc]]
C.-Y. Zhang, P.-C. Li, and M. Guo, *Greybody factor and power spectra of the Hawking radiation in the novel 4D Einstein-Gauss-Bonnet de-Sitter gravity*, Eur. Phys. J. **C 80** (2020) 874; [arXiv:2003.13068 [hep-th]]
S.-W. Wei and Y.-X. Liu, *Extended thermodynamics and microstructures of four-dimensional charged Gauss-Bonnet black hole in AdS space*, Phys. Rev. **D 101** (2020) 104018; [arXiv:2003.14275 [gr-qc]]
S.U. Islam, R. Kumar, and S.G. Ghosh, *Gravitational lensing by black holes in the 4D Einstein-Gauss-Bonnet gravity*, J. Cosmo. Astropart. Phys. **09** (2020) 030; [arXiv:2004.01038 [gr-qc]]
R.A. Konoplya and A.F. Zinhailo, *Grey-body factors and Hawking radiation of black holes in 4D Einstein-Gauss-Bonnet gravity*, Phys. Lett. **B 810** (2020) 135793; [arXiv:2004.02248 [gr-qc]]
L. Ma and H. Lu, *Vacua and exact solutions in lower D limits of EGB*, Eur. Phys. J. **C 80** (2020) 1209. [arXiv:2004.14738 [gr-qc]]
- [15] R.A. Konoplya and A.F. Zinhailo, *Quasinormal modes, stability and shadows of a black hole in the novel 4D Einstein-Gauss-Bonnet gravity*, arXiv:2003.01188 [gr-qc];
M.S. Churilova, *Quasinormal modes of the Dirac field in the novel 4D Einstein-Gauss-Bonnet gravity*, arXiv:2004.00513 [gr-qc];
A.K. Mishra, *Quasinormal modes and Strong Cosmic Censorship in the novel 4D Einstein-Gauss-Bonnet gravity*, Gen. Relat. Grav. **52** (2020) 106; [arXiv:2004.01243 [gr-qc]]
A. Aragón, R. Bécar, P.A. González, and Y. Vásquez, *Perturbative and nonperturbative quasinormal modes of 4D Einstein-Gauss-Bonnet black holes*, Eur. Phys. J. **C 80** (2020) 773; [arXiv:2004.05632 [gr-qc]]
X.-X. Zeng, H.-Q. Zhang, and H. Zhang, *Shadows and photon spheres with spherical accretions in the four-dimensional Gauss-Bonnet black hole*, Eur. Phys. J. **C 80** (2020) 872; [arXiv:2004.12074 [gr-qc]]

- M.S. Churilova, *Quasinormal modes of the test fields in the novel 4D Einstein-Gauss-Bonnet-de Sitter gravity*, arXiv:2004.14172 [gr-qc].
- [16] S.-W. Wei and Y.-X. Liu, *Testing the nature of Gauss-Bonnet gravity by four-dimensional rotating black hole shadow*, arXiv:2003.07769 [gr-qc].
- [17] J.-X. Feng, B.-M. Gu, and F.-W. Shu, *Theoretical and observational constraints on regularized 4D Einstein-Gauss-Bonnet gravity*, Phys. Rev. **D 103** (2021) 064002. [arXiv:2006.16751 [gr-qc]]
- [18] S.-J. Yang, J.-J. Wan, J. Chen, J. Yang, and Y.-Q. Wang, *Weak cosmic censorship conjecture for the novel 4D charged Einstein-Gauss-Bonnet black hole with test scalar field and particle*, Eur. Phys. J. **C 80** (2020) 937. [arXiv:2004.07934 [gr-qc]]
- [19] X.-H. Ge and S.-J. Sin, *Causality of black holes in 4-dimensional Einstein-Gauss-Bonnet-Maxwell theory*, Eur. Phys. J. **C 80** (2020) 695. [arXiv:2004.12191 [hep-th]]
- [20] Y.-F. Cai, C. Lin, B. Wang, and S.-F. Yan, *Sound speed resonance of the stochastic gravitational wave background*, Phys. Rev. Lett. **126** (2021) 071303. [arXiv:2009.09833 [gr-qc]]
- [21] P.C.W. Davies, *The thermodynamic theory of black holes*, Proc. Roy. Soc. Lond. **A 353** (1977) 499; P.C.W. Davies, *Thermodynamics of black holes*, Rept. Prog. Phys. **41** (1978) 1313.
- [22] C. Lan, Y.-G. Miao, and H. Yang, *Quasinormal modes and thermodynamics of regular black holes*, Nucl. Phys. **B 971** (2021) 115539. [[arXiv:2008.04609 [gr-qc]]]
- [23] H.P. Nollert, *Quasinormal modes: The characteristic ‘sound’ of black holes and neutron stars*, Class. Quant. Grav. **16** (1999) R159;
K.D. Kokkotas and B.G. Schmidt, *Quasi-normal modes of stars and black holes*, Living Rev. Relativ. **2** (1999) 2; [arXiv:gr-qc/9909058]
E. Berti, V. Cardoso, and A.O. Starinets, *Quasinormal modes of black holes and black branes*, Class. Quant. Grav. **26** (2009) 163001; [arXiv:0905.2975 [gr-qc]]
R.A. Konoplya and A. Zhidenko, *Quasinormal modes of black holes: From astrophysics to string theory*, Rev. Mod. Phys. **83** (2011) 793. [arXiv:1102.4014 [gr-qc]]
- [24] V. Cardoso, A.S. Miranda, E. Berti, H. Witek, and V.T. Zanchin, *Geodesic stability, Lyapunov exponents and quasinormal modes*, Phys. Rev. **D 79** (2009) 064016. [arXiv:0812.1806 [hep-th]]
- [25] R.A. Konoplya and Z. Stuchlík, *Are eikonal quasinormal modes linked to the unstable circular null geodesics?*, Phys. Lett. **B 771** (2017) 597; [arXiv:1705.05928 [gr-qc]]
F. Moura and J. Rodrigues, *Eikonal quasinormal modes and shadow of string-corrected d-dimensional black holes*, Phys. Lett. **B 819** (2021) 136407. [arXiv:2103.09302 [hep-th]]
- [26] V. Perlick, O.Y. Tsupko, and G.S. Bisnovatyi-Kogan, *Influence of a plasma on the shadow of a spherically symmetric black hole*, Phys. Rev. **D 92** (2015) 104031; [arXiv:1507.04217 [gr-qc]]
K. Jusufi, *Quasinormal modes of black holes surrounded by dark matter and their connection with the shadow radius*, Phys. Rev. **D 101** (2020) 084055. [arXiv:1912.13320 [gr-qc]]

- [27] S. Chandrasekhar, *The mathematical theory of black holes*, Oxford University Press, New York, 1983.
- [28] J. Arrechea, A. Delhom, and A. Jiménez-Cano, *Inconsistencies in four-dimensional Einstein-Gauss-Bonnet gravity*, Chinese Phys. **C 45** (2021) 013107. [arXiv:2004.12998 [gr-qc]]
- [29] R. Wald, *Gedanken experiments to destroy a black hole*, Ann. Phys. **82** (1974) 548.
- [30] R. Brito, V. Cardoso, and P. Pani, *Superradiance*, Lecture Notes in Physics **971** (2020). [arXiv:1501.06570 [gr-qc]]